Molecular dynamics simulations of supported metal nanocatalyst formation by plasma sputtering

Reference:

Brault Pascal, Neyts Erik.- Molecular dynamics simulations of supported metal nanocatalyst formation by plasma sputtering
Catalysis today - ISSN 0920-5861 - 256:1(2015), p. 3-12
DOI: http://dx.doi.org/doi:10.1016/j.cattod.2015.02.004
Handle: http://hdl.handle.net/10067/1274080151162165141

Molecular dynamics simulations of supported metal nanocatalyst formation by plasma sputtering

Pascal Brault[1] and Erik C. Neyts[2]

[1]GREMI, UMR7344 CNRS Université d'Orléans BP6744, 45067 Orléans Cedex 2, France

[2]Department of Chemistry, Research Group PLASMANT, University of Antwerp, BE-2610 Antwerp-Wilrijk, Belgium

Corresponding author: Pascal Brault, +33(2)38417125, pascal.brault@univ-orleans.fr

Abstract

Magnetron sputtering is a widely used physical vapor deposition technique for deposition and formation of nanocatalyst thin films and clusters. Nevertheless, so far only few studies investigated this formation process at the fundamental level. We here review atomic scale molecular dynamics simulations aimed at elucidating the nanocatalyst growth process through magnetron sputtering. We first introduce the basic magnetron sputtering background and machinery of molecular dynamics simulations, and then describe the studies conducted in this field so far. We also present a perspective view on how the field may be developed further.

Keywords: molecular dynamics; supported nanocatalyst; sputter deposition; supported cluster growth

1. Introduction

Magnetron plasma sputter deposition is a well-established deposition technique that is widely used in research and industry [1]. It can be used as an atom or cluster source [2-3] for which composition, kinetic energies and angle distributions (more or less peaked) are well defined. Due to the atomic nature of the plasma sputtering process, deposition of thin films in the form of supported clusters of well-defined composition, structure and morphology has become possible. This is highly important in catalysis, where fabrication processes that precisely meet such requirements are highly demanded [4]. Heterogeneous catalysis is typically concerned with supported assemblies of nano-sized particles, dispersed on a support with a large surface area [5, 6]. Due to the complexity of the catalyst formation process, predictions of the size, morphology and atomic structure of the supported catalyst clusters is a very challenging task. Computer simulations may therefore prove to be very useful in delivering precisely such data.

Molecular dynamics (MD) is a computer simulation technique in which the system evolution is followed at the atomic level and hence, MD is well suited to describe materials at the atomic scale [7-12]. Since magnetron sputter deposition is an atomic process, MD simulations are the tool par excellence to investigate the involved growth process [13-20]. However, until now, MD simulations have not often been applied for investigating catalyst synthesis in general and catalyst synthesis by magnetron sputtering and other physical vapour deposition processes in specific, in part due to the complexity of the process. Such simulations, on the other hand, have often been used for the determination of equilibrium structures, and the study and effects of catalytic reactions, also in the context of a plasma environment [21-22].

In this contribution we will therefore focus on the capabilities of MD for predicting the growth of nanocatalysts by magnetron sputtering. First, we will describe the input parameters of MD simulations and pay specific attention to crucial issues such as energy distributions and transfer of high energy particles (0.1 to 10s eV). Subsequently, we will elaborate on the growth of platinum nanocatalyst particles based on MD simulations. We will also provide a perspective on how the field may be developed further. Finally a conclusion will be given.

2. Molecular dynamics simulations for magnetron sputtering

We first briefly recall the main features of magnetron sputtering as an atom or cluster source. Basically, a plasma of the buffer gas (typically argon) is created by a direct current or a radiofrequency power supply applied to an electrode located inside a vacuum chamber. The pressure is typically in the range 0.01 Pa to 100 Pa. As the electrode is usually negatively biased (usually in the range from 100 to 1000 V), positive ions of the buffer gas are bombarding the electrode, now called the target, containing the catalyst. Since typical sputtering thresholds are around 20 eV, such ion bombardment results in the ejection of atoms from the target. These sputtered atoms will travel from the target through the plasma to the substrate and eventually deposit on the substrate surface. During the transport of the sputtered material through the plasma, the energy distribution of the sputtered atoms will change due to collisions with the buffer gas atoms, which in turn depends on the buffer gas pressure. If the pressure is sufficiently high, the sputtered atoms show a relatively high self-collision probability and start to form clusters in the plasma phase. This phenomena is called gas condensation and is the basis of the design of nanocluster beam sources [3]. The energy distribution function of the sputtered atoms leaving the target can be approximated by the so-called Thomson formula [23-25]:

$$f(E) \propto \frac{1-\left(\frac{E_{coh}+E}{\gamma E_{Ar^+}}\right)^{\frac{1}{2}}}{E^2\left(1+\frac{E_{coh}}{E}\right)^3} \quad (1)$$

where E_{coh} is the cohesive energy of the target material, E is the energy of the ejected atoms, γ is the kinetic energy mass transfer factor, and E_{Ar+} is the kinetic energy of the impinging Ar-ions.

The final energy after collisions along the path from target to substrate of a sputtered atom with energy E when leaving the target is given by [25]:

$$E_F = \left(E - k_B T_g\right)\exp\left[n\ln\left(E_f / E_i\right)\right] + k_B T_g$$

Here, $E_f/E_i = 1-\gamma/2$ is the ratio of energies after and before a collision [26]. The kinetic energy mass transfer factor is defined as:

$$\gamma = 4\frac{m_g m_s}{(m_g + m_s)^2}$$

where m_g and m_s are gas/plasma phase atom (e.g. argon) and sputtered atom masses, respectively. The number of collisions that take place in the gas is given by:

$n=dP\tau/kBT_g$

where T_g is the sputtering gas temperature, d is the travelled distance, P is the sputtering gas pressure, and τ is the collision cross section assuming hard-core interactions. In order to calculate the energy loss (E_F) of sputtered atoms with the gas atoms, a Maxwell-Boltzmann (MB) distribution at T_g is assumed for the gas. In most sputter deposition sources this corresponds to T_g = 300 K and E_g = kBT_g. Because we search for the complete energy distribution of sputtered atoms, for each E_g in the Maxwell-Boltzmann energy distribution for the gas, the energy loss is calculated for a fixed value of the kinetic energy E of a sputtered atom. This is repeated for each E in the Thompson distribution and weighted by the collision probability, which is simply the convolution of $f(E)$ and the MB distribution at T_g [25]. Initial velocities or equivalently kinetic energies can be readily obtained from such a distribution. The velocities of the sputtered atoms can also be sampled from a Maxwell-Gaussian distribution with a mean kinetic energy corresponding to the energy loss calculated from Equation (1) with randomly selected incident angles. In figure 1, we show a typical energy distribution for Pt sputtered at various Ar pressures P for a given target-to-substrate distance and impinging Ar^+ ion energy on the target.

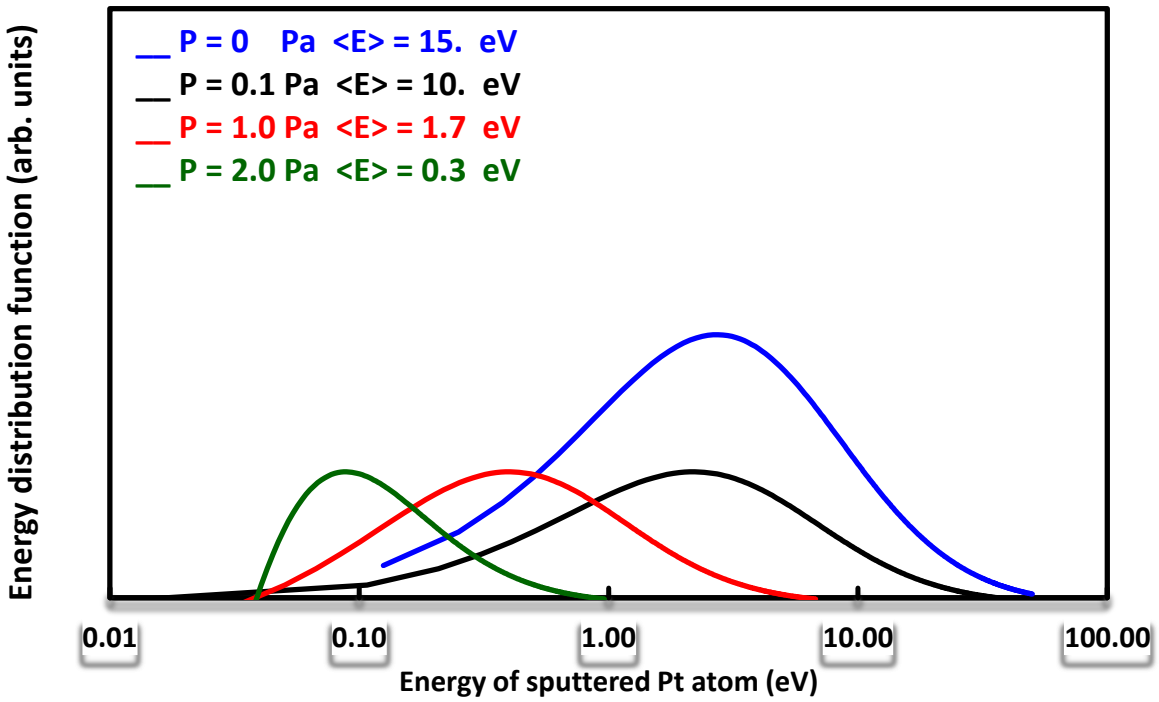

Figure 1: Example of energy distribution functions of Pt atoms arriving at the substrate located at 10 cm from the sputtered target biased at 300 V. Plots are given for different Ar pressures *P* (log scale for the abscissae).

MD simulations make use of this information by randomly selecting initial velocities from such distribution functions, while the initial positions of atoms arriving at the substrate are typically randomly chosen in {*x,y*}-directions and chosen to be beyond the interaction range of the interaction potential used in the *z*-direction.

In practice, MD simulations of the sputter deposition process require integrating the Newton equations of motion for the assembly of incoming atoms (or molecules or clusters) as well as the substrate atoms. As the substrate atoms' trajectories are also explicitly followed through space and time, the response of the substrate to individual atom impacts can be monitored as well.

The Newton equation of motion reads:

$$\frac{\partial^2 \vec{r}_i(t)}{\partial t^2} = \frac{1}{m_i}\vec{f}_i, \quad \text{with the force } \vec{f}_i = -\frac{\partial}{\partial \vec{r}} V(\vec{r}_1(t), \vec{r}_2(t), \cdots, \vec{r}_N(t)) \qquad (2)$$

where $\vec{r}_i(t)$ is the instantaneous position of atom i with mass m_i at time t, and V is the potential energy function governing all interatomic interactions.

Solving this equation thus requires the availability of a suitable interatomic interaction potential *V*. For metal catalysts many-body potentials are required and constructing suitable potentials (especially for accurately describing the metal-support interactions), is an active field of research [27-29]. As we will describe in the perspective section, we believe this is an important field of development for advancing theoretical studies of plasma sputter deposition.

A class of potentials often used for describing catalyst evolution under various conditions is the Embedded Atom Model (EAM) [30-33]. The EAM potential is based on a concept borrowed from

density functional theory stipulating that in general the energy of a solid is a unique functional of the electron density. The embedded-atom method uses the concept of electron (charge) density to describe metallic bonding. Essentially, each atom contributes through a spherical, exponentially-decaying field of electron charge, centered at its nucleus, to the overall charge density of the system. Binding of atoms is modelled as embedding these atoms in this "pool" of charge, where the energy gained by embedding an atom at location *r* is some function of the local density. Various collections of EAM parameters of metals of interest for catalysis, and for their alloys have been developed by Zhou et al [32] and Lin et al [33].

The EAM potential energy E_{pot} of the system can be expressed as:

$$E_{pot} = \sum_{i=1}^{N} E_i = \frac{1}{2}\sum_{i=1}^{N}\sum_{i,j,i\neq j}^{N}\phi_{ij}\left(r_{ij}\right) + \sum_{i=1}^{N} F_i\left(\rho_i\right) \tag{3}$$

where E_i is the potential energy of an atom *i*, $\phi(r_{ij})$ is the pair energy term as a function of the interatomic distance r_{ij} between atoms *i* and *j*, and $F_i(\rho_i)$ is the many-body embedding energy term as a function of the local electron density, ρ_i, at the position of atom *i*. The local electron density is calculated as a linear sum of the partial electron density contributions from the neighboring atoms:

$$\rho = \sum_{j,j\neq 1}^{N} f_i\left(r_{ij}\right) \tag{4}$$

where $f_j(r_{ij})$ is the contribution from atom *j* to the electron density at the site of the atom *i*. The pair energy term is defined as:

$$\phi\left(r\right) = \frac{A\exp\left[-\alpha\left(\frac{r}{r_e}-1\right)\right]}{1+\left(\frac{r}{r_e}-\kappa\right)^{20}} - \frac{B\exp\left[-\beta\left(\frac{r}{r_e}-1\right)\right]}{1+\left(\frac{r}{r_e}-\lambda\right)^{20}} \tag{5}$$

where r_e is the equilibrium spacing between nearest neighbors, *A*, *B*, *α*, and *β* are four adjustable parameters, and *κ* and *λ* are two additional parameters for the cutoff distances. The electron density function is taken to have the same form as the attractive term in the pair potential with the same values.

The electron density function is given by:

$$f\left(r\right) = \frac{f_e\exp\left[-\beta\left(\frac{r}{r_e}-1\right)\right]}{1+\left(\frac{r}{r_e}-\lambda\right)^{20}} \tag{6}$$

The pair potential between atoms of two different elements (*a* and *b*) is then constructed as:

$$\phi^{ab}\left(r\right) = \frac{1}{2}\left[\frac{f^b\left(r\right)}{f^a\left(r\right)}\phi^{aa}\left(r\right) + \frac{f^a\left(r\right)}{f^b\left(r\right)}\phi^{bb}\left(r\right)\right] \tag{7}$$

The embedding energy function is represented by three equations defining it in different electron density ranges and having matching values and slopes at the two junctions,

$$F(\rho)=\sum_{i=0}^{3}F_{ni}\left(\frac{\rho}{0.85\rho_e}-1\right)^i, \quad \rho<0.85\rho_e \tag{8}$$

$$F(\rho)=\sum_{i=0}^{3}F_{i}\left(\frac{\rho}{\rho_e}-1\right)^i, \quad 0.85\rho_e\le\rho<1.15\rho_e \tag{9}$$

$$F(\rho)=F_n\left[1-\eta\ln\left(\frac{\rho}{\rho_s}\right)\right]\left(\frac{\rho}{\rho_s}\right)^{\eta}, \quad \rho\ge1.15\rho_e \tag{10}$$

Many-body empirical potentials, including Modified EAM and tight-binding potentials, can also be used for studying properties of catalytic metals and their alloys [34-39]. These potentials are very close in nature to the EAM family.

The study of supported nanocatalysts, however, also requires an interaction potential for describing the supporting material. The most often encountered catalyst supports and for which there are tested potentials available are carbons [40-45] and metal oxides (including a.o. TiO_2 [29, 46-51], Al_2O_3 [52-54], SiO_2 [55-59] and MgO [13, 14, 60-61]), in the form of single or multiwall nanotubes, nano- or micropowders, thin films, or other forms.

More critical, however, is the metal-support interaction potential. The continuous developments in density functional theory calculations allowed considerable progress to be made in this field [62]. Moreover, fitting analytic interaction potentials to DFT data allows to conduct extended classical molecular dynamics simulations, while ab-initio molecular dynamics studies remain time consuming and limited to rather small systems. Nevertheless, some systems have been studied and some interaction potentials have been proposed. Examples include Pt-carbon for, e.g., fuel cells [28, 63-67], metal-carbon for plasma catalysis [68-70] and nanotube growth [71-74]. Pt interactions with Al_2O_3 and SiO_2 have also been studied, although to a lesser extent [75,76], as well as Pd on MgO and Al_2O_3 [77,78].

3. MD simulations of catalyst nanoparticle growth by sputtering

So far, only a limited number of studies have been reported on simulation of the deposition and growth of catalyst nanoparticles or nanofilms through sputtering. Most studies, including most of the works cited above [28, 63-78], either focus on the reactivity of such clusters or on the structure of the clusters, as a function of the substrate structure and its temperature, and not on the actual deposition or growth process. Nevertheless, the studies available so far allows us to identify a number of trends, and demonstrate the usefulness of conducting MD simulations of nanocatalyst growth in the context of physical magnetron sputtering.

As already pointed out in the preceding section, the main interest of magnetron sputtering is to act as an atom source with a controllable energy distribution function [79]. As a first example, Inoue et al. employed detailed molecular dynamics simulations to study Au and Ni cluster deposition onto single wall carbon nanotubes (both vertically aligned and lying on a substrate) [80]. The goal of the study was to determine the mechanism and the preferred site of cluster anchoring on the nanotube. An interesting feature emerging from these simulations was the change in morphology as the cluster is gradually wetting the surface. In Figure 2, both Au and Ni clusters are seen to coalesce, which

results in the formation of larger clusters. Moreover, the simulations indicate that some metal atoms are desorbing back into the vapor, as they are unable to find a suitable binding site to anchor to the cluster. The conclusion was therefore drawn that the adsorption of the cluster on the nanotube array may potentially require concurrent cluster atom ejection from the cluster.

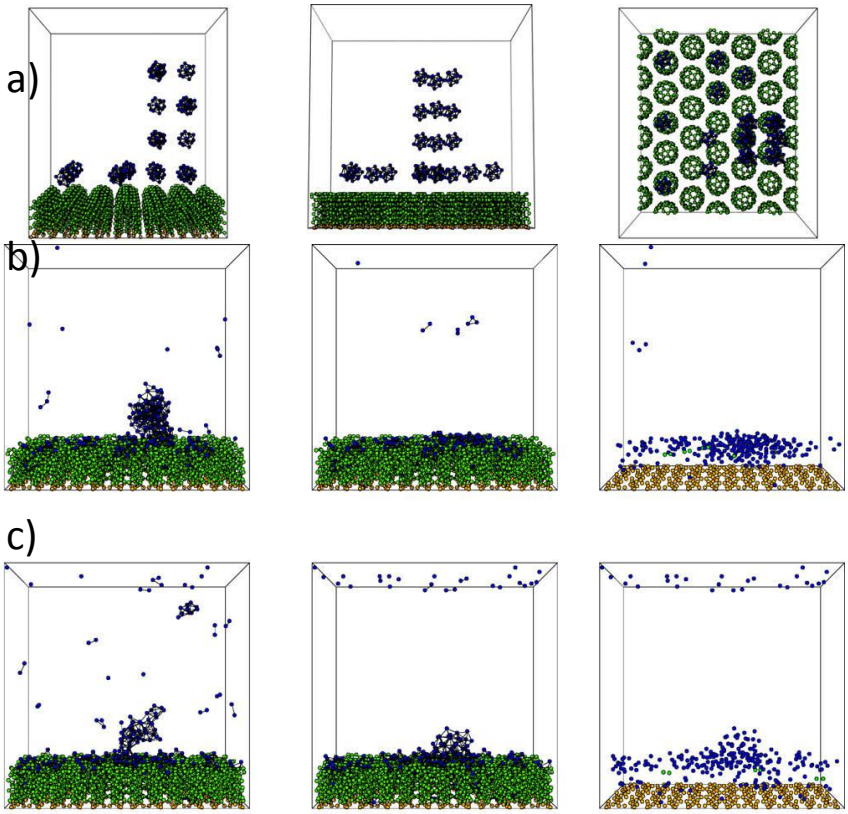

Figure 2: Vapor deposition of Ni and Au clusters on vertically aligned carbon nanotubes. a) Geometry of the deposition. View from x, y, z directions (from left to right). b) deposition of nickel clusters. c) deposition of gold clusters. In the right column, the nanotubes have been removed for better visualization of the metal atom arrangements (Reprinted from Ref. 80, Elsevier).

Recent work on sputtered Pt atom deposition on vertical single wall carbon nanotube arrays [81] highlights the role of the kinetic energy distribution function on the clustering, structure and morphology of the adsorbed Pt. Note that due the periodic boundary conditions in the horizontal plane, the simulation of a single nanotube corresponds to simulating a square array of nanotubes.

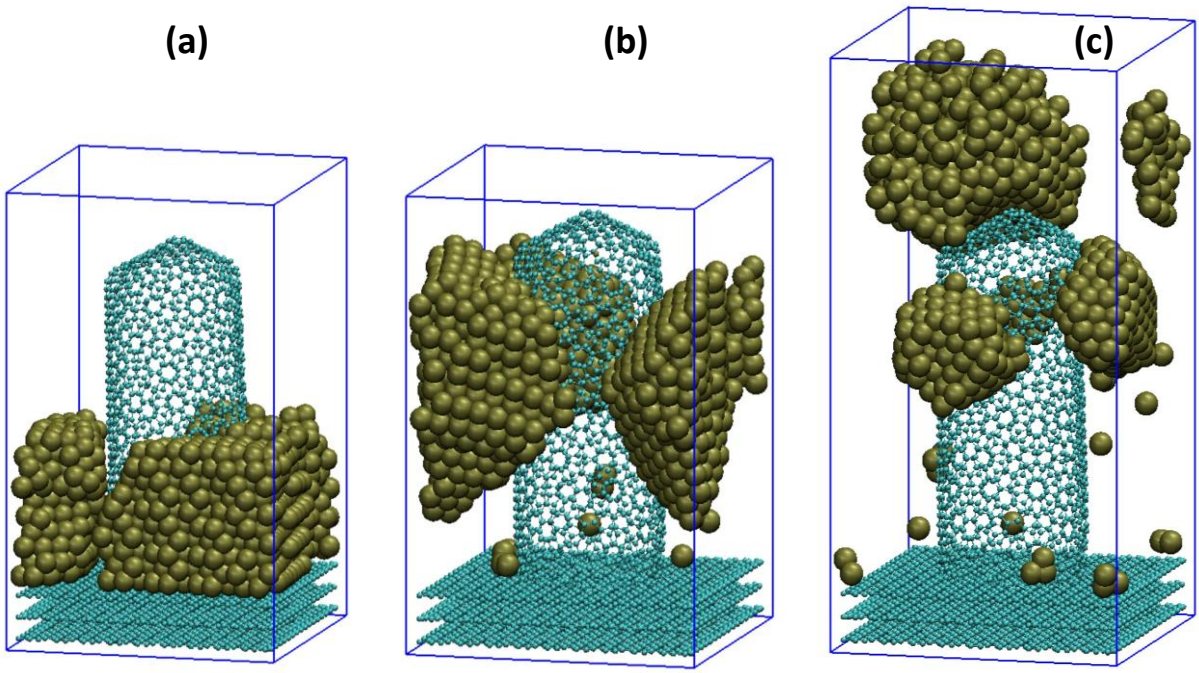

Figure 3: Schematic picture of Pt deposition on CNTs. the mean kinetic Pt energy is (a) 1 eV, (b) 0.1 eV and (c) 0.026 eV. ●C and ●Pt (Adapted from Ref. 81)

The effect of the kinetic energy distribution of the impacting Pt-atoms is clearly observed in figure 3, showing how this kinetic energy is affecting both diffusion of Pt along the nanotube as well as the morphology of the Pt-cluster. The higher the Pt-energy, the closer to the nanotube base the cluster will form. When lowering the incoming energy, a transition from flat film growth (Fig. 3(a)) to a large cluster (Fig. 3(b)), and eventually the formation of dispersed Pt clusters close to the nanotube tip at thermal energy (300 K) is observed. Moreover, the crystallinity of the clusters is reduced at low kinetic energy. Indeed, as shown in Figure 4, the calculated XRD patterns of Pt-nanoclusters, corresponding to the atomic arrangements of Figure 3, show less pronounced crystallinity features with decreasing energy.

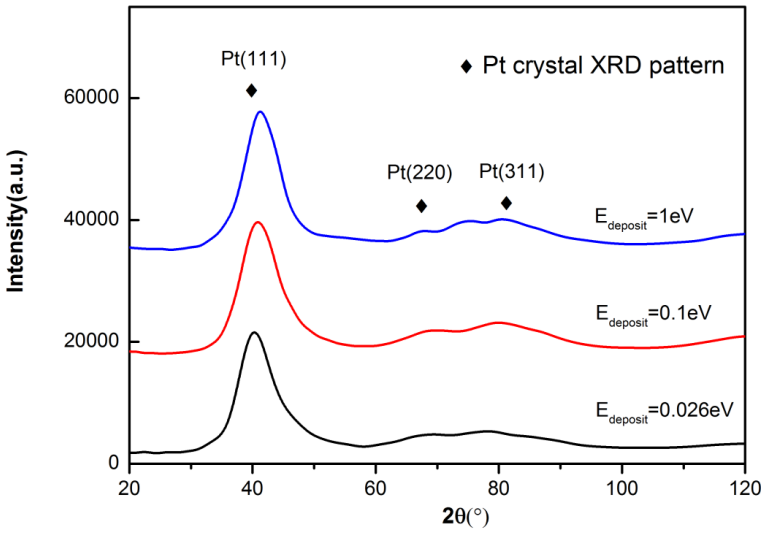

Figure 4: Calculated X-Ray diffraction patterns of platinum clusters from Figure 3, at the three different energies. (Reprinted from Ref. 81)

In the same spirit, Pt deposition was also simulated on a model porous carbon for mimicking Pt sputter deposition onto a fuel cell porous carbon electrode [17]. For validating the platinum-carbon potential, MD simulations were carried out using two different pair potentials as determined from fitting both Pt-graphite experimental data [63,64] and data calculated at the DFT level [66,67]. The latter was found to more accurately reproduce the experimental evidence on the growth of amorphous Pt clusters. The obtained films are shown in figure 5. It can be seen from the figure, that for all three investigated kinetic energies, film-like thin films with nanofeatures are formed, and the film morphology closely follows the substrate morphology. The Pt-atoms are also observed to penetrate the amorphous carbon pores, in good agreement with experiments [17, 82-84].

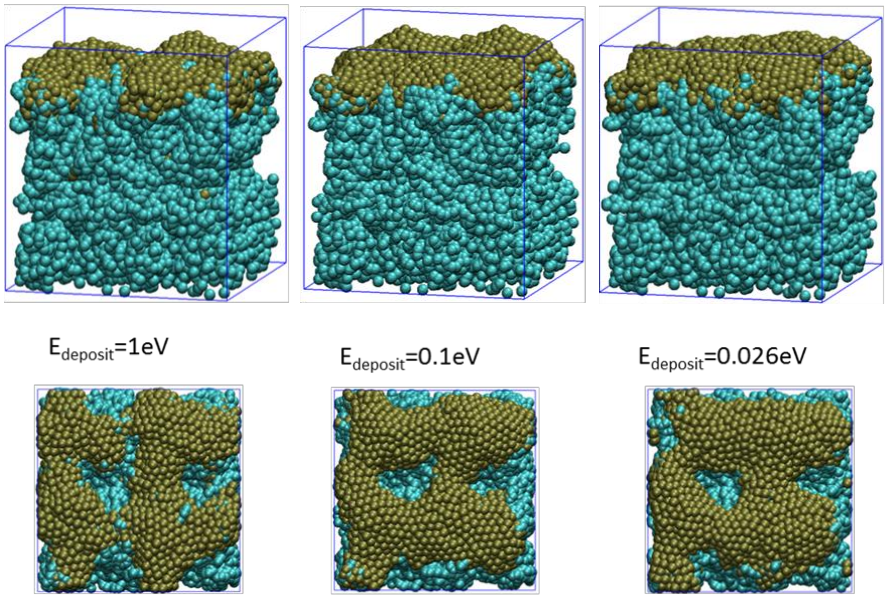

Figure 5: Snapshots of Pt deposition on the porous carbon substrate at various impinging mean kinetic energies. The green spheres represent C-atoms and the brownish spheres represent Pt-atoms (Reprinted from Ref. 17, Elsevier)

MD simulations of Pd deposition onto a α-Al_2O_3 crystal demonstrated that adsorbed Pd particles are 3D clusters [78], in agreement with the expected 3D Volmer-Weber growth mechanism for this system. Structural analysis shows a cubic packing of the microcrystals. These microcrystals are pyramid-shaped, truncated by the (111) plane and exhibiting (111) and (100) facets. These simulation results are in excellent agreement with STM measurements [85]. Moreover, the supported particles were found to be stable at low and moderate temperatures. Above 500 K, the Pd atoms start to penetrate into the substrate (Figure 6), leading to a loss in crystallinity, and correlated with the loss of catalytic activity with increasing temperature [86].

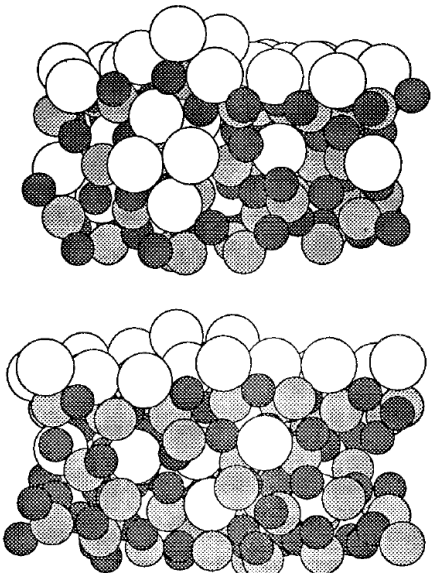

Figure 6: MD simulation of Pd cluster atoms (large white spheres) penetrating into a Al_2O_3 substrate (Reprinted from Ref. 78, American Chemical Society)

In a study by Haberland *et al.*, molecular dynamics simulations were employed to study deposition of clusters at hyperthermal energy [19, 20]. At low incoming energies, it was found that the clusters do not sufficiently wet the surface, leading to poor adhesion. In this case, the deposited catalyst particle will be very mobile and sintering will inevitably occur, leading to a loss of catalytic activity. Increasing the deposition energy, however, leads to flattening of the cluster, and subsequent penetration and melting of the cluster into the substrate. This process is shown in Figures 7 and 8. Hence, such MD simulations allow to define suitable energy windows for optimal film growth.

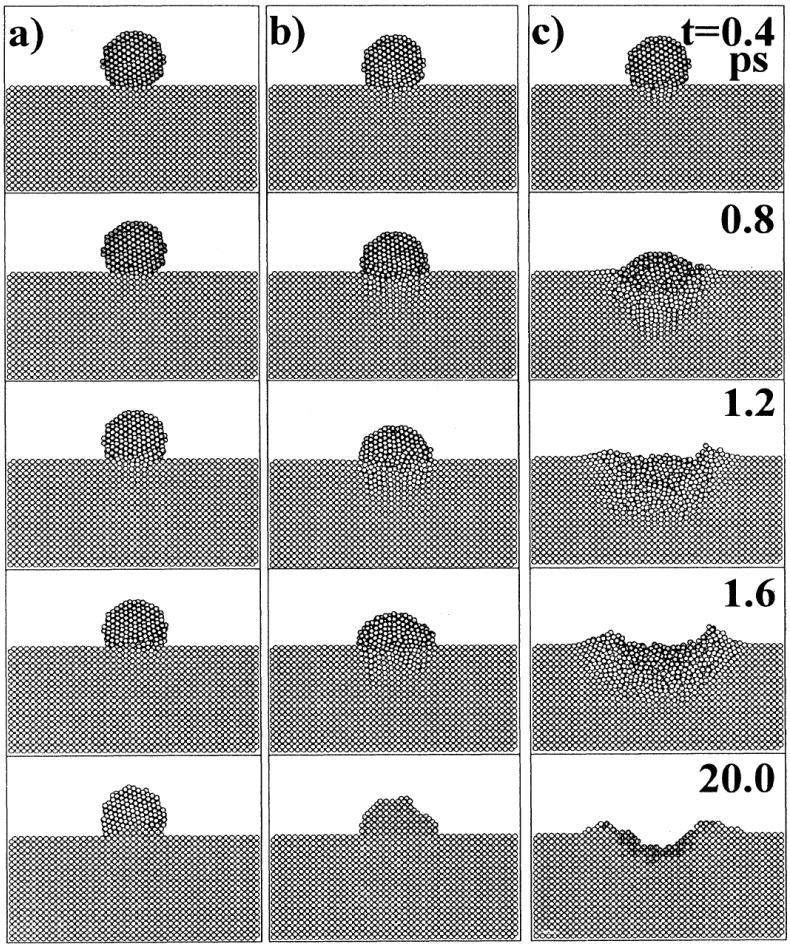

Figure 7: Time resolved snapshot of a Mo_{1043} cluster with (a) 0.1 eV, (b) 1 eV, and (c) 10 eV kinetic energy per atom impinging on a Mo(001) surface. A three-atom-deep cut through the surface is shown. Note the shock wave propagating into the surface for the 10-eV collision (Reprinted from Ref. 20, American Physical Society).

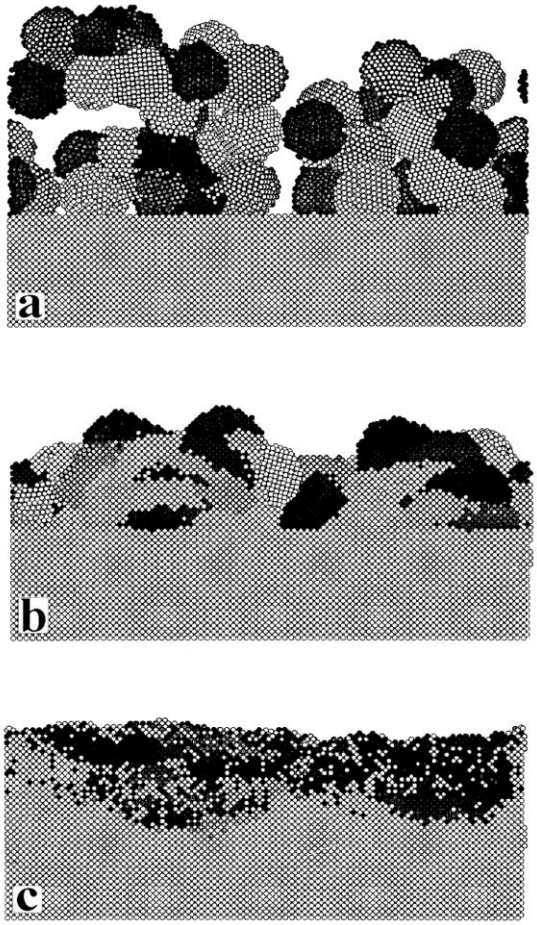

Figure 8: Snapshots of cluster deposition simulated by molecular dynamics. Different thin film morphologies are found as function of cluster impact energy: (a) 0.1 eV/atom (b) 1 eV/atom, (c) 10 eV/atom (collision (Reprinted from Ref. 20, American Physical Society).

It is thus clear that MD simulations of sputtered catalyst deposition provide very useful information at the atomic level both on the resulting catalyst structure (crystalline vs. amorphous), morphology (two- or three-dimensional), and the importance of the support material and the kinetic energy of impinging particles. Moreover, the availability of accurate interaction potentials obtained either from fitting quantum mechanical data or other semi-empirical methods allows to compare to experiments, including XRD, transmission electron microscopy (TEM) and extended x-ray absorption fine structure measurements. In the latter case, the measurements can be directly compared to the calculated radial distribution functions.

4. Future perspective

Despite the increasing interest in MD simulations for describing catalyst growth and reactivity, many issues remain unresolved. In our opinion, obtaining a more fundamental understanding of catalyst nanoparticle growth by sputter deposition requires an integrated approach, combining simulations and experiments. We currently envisage two main directions for near-future studies. First, accurate reactive potentials capable of describing not only the catalytic material but also the metal – support interactions are urgently required to study the deposition and growth process at the atomic scale and unravel the underpinning deposition mechanisms. Second, the systematic experimental study in reducing the use of platinum by combination with other metals, such as Pd, Au, and including common metals, such as Fe, Ni, or Cu.

4.1 Development of reactive potentials for catalysts and catalyst – support interactions

As is clear from the discussion above, atomic scale reactive molecular dynamics simulations may provide a fundamental insight in the deposition process. As discussed in section 2, however, such simulations require an interatomic potential capable of accurately representing the studied system.

In practice, developing parametrizations for interatomic potentials, intended to be used in reactive molecular dynamics simulations, turns out to be a very tedious task. Ideally, the potential should be able to describe any possible interaction between any pair, triplet, quadruplet or higher order interactions of the elements included in the parametrization. This is a formidable task, and therefore reactive potentials are typically developed for a specific class of material.

Hence, a wide variety of different functional forms have been developed, corresponding to specific material classes. Examples include, among others, the EAM, Finnis-Sinclair and analytical tight-binding potentials for metals [30-39], MEAM for metals and covalent materials [53-54], Tersoff-type and Brenner-type potentials for covalent materials [40-44] or Coulomb/Buckingham potentials for ionic materials [13, 14, 46, 47, 52, 60].

A functional form suitable for describing only a single class of materials is often insufficient in the context of sputter deposition of a catalyst on a support, as typically the catalyst material is a metal and the support a metal oxide or a covalent material such as carbon. Moreover, the actual catalytic process often also involves oxygen, hydrogen and/or hydrocarbons. Hence, more general descriptions of the interatomic interactions are generally required.

Some potentials, such as the MEAM [53,54], COMB [51,58] and ReaxFF [45, 68-74] families, are indeed intended to be of a generic nature, in the sense that they are in principle capable of modeling any material, and not be confined to a specific class of materials, provided at least a suitable parametrization is developed. While a large number of elemental atom types can nowadays indeed be modeled using these potentials, constructing parametrizations for combinations of elements turns out to be more complex. In the context of combined catalyst / support systems, examples of available parametrizations include the COMB parametrization for {Si, Cu, Hf, Ti, O, their oxides and Zn, Zr and U} [51], and for {H, C, N, O, Cu, Ti, Zn, Zr} [58], MEAM parametrizations for {Al, Si, Mg, Cu and Fe alloys} [53, 54], and a variety of binary and ternary Pt-alloys [53, 54, 87], and ReaxFF parametrizations for {Bi/Mo/O} [88] and {Mo,V,O} [89].

With continuous further development of reactive potentials, a larger variety of catalyst / support combinations will come within reach of atomic scale molecular dynamics simulations.

4.2 Multimetallic catalysts

As an example of MD simulations of multimetallic catalysts, we here highlight our latest results on sputter deposition of a trimetallic catalyst, which is of interest for reducing the Pt content in fuel cell cathodes for oxygen reduction [90-92]. Figures 9 and 10 display the atomic structure of the catalyst film at different deposition times for simultaneous co-sputtering of Pd, Pt and Au atoms and co-sputtering of Pd, Au followed by Pt sputtering, respectively.

a)

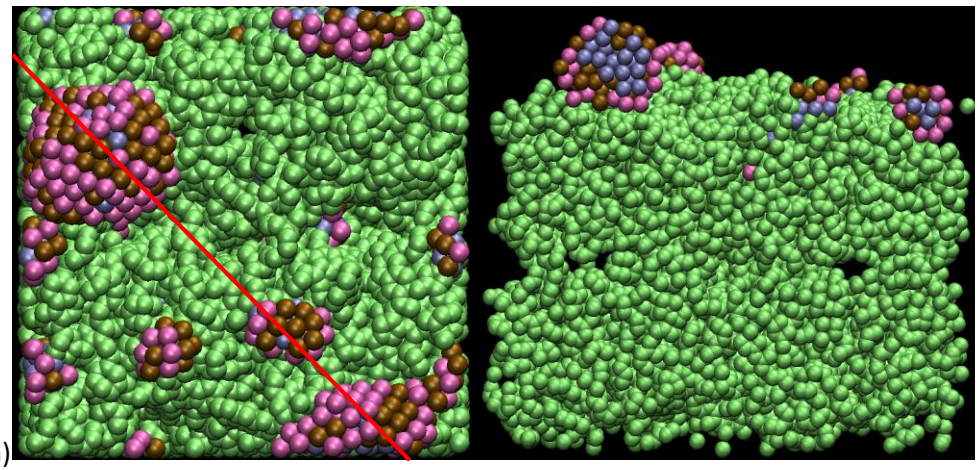

b)

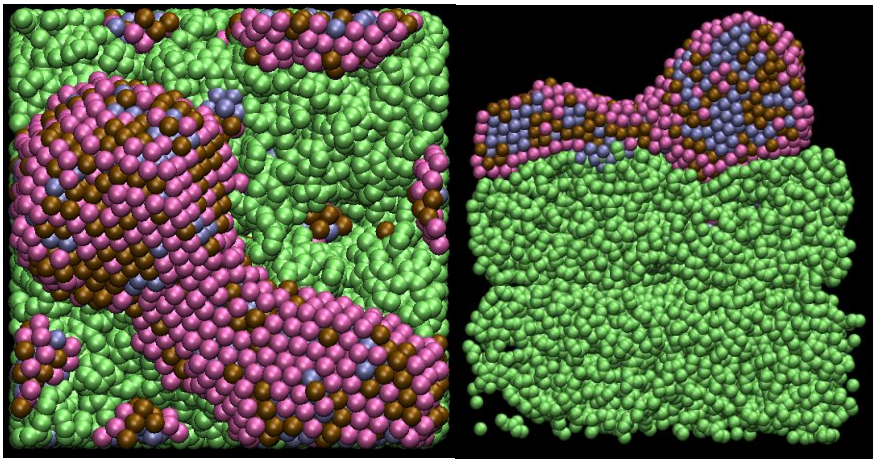

Figure 9: Co-sputtering deposition of Pd, Pt and Au atoms before (a) and after (b) coalescence; the cross sectional view is made along the red line. ●C, ●Pd, ●Pt, ●Au

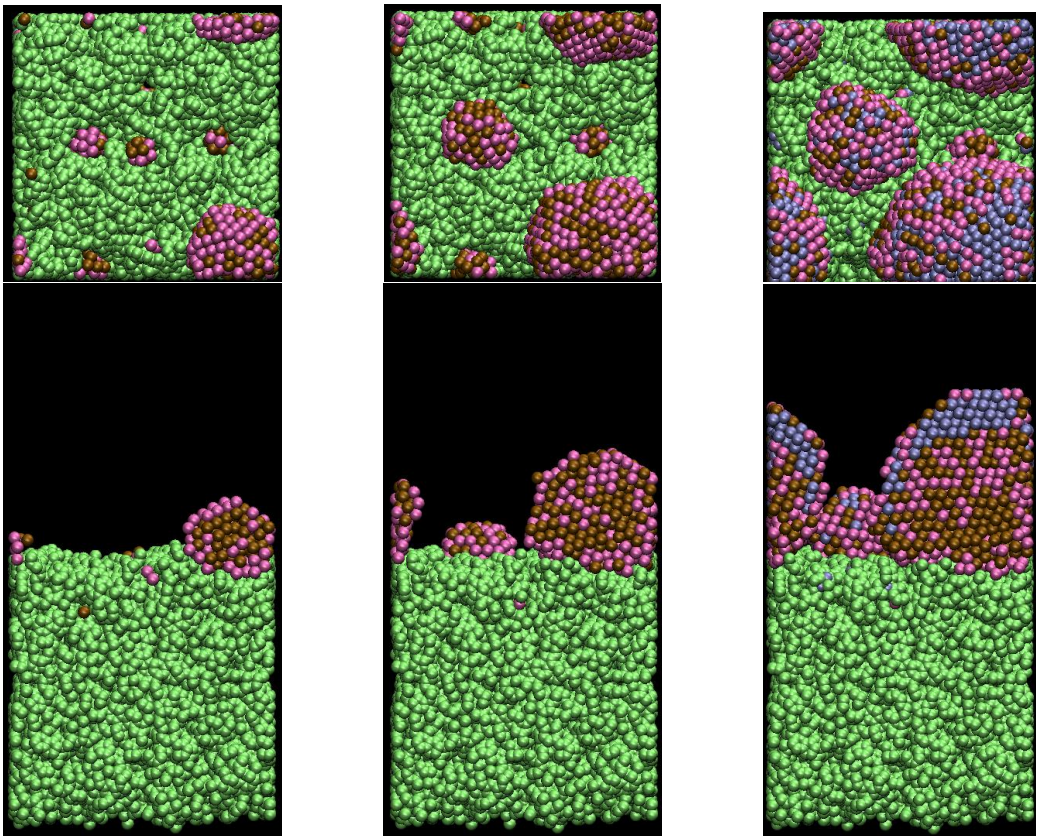

Figure 10: Top and side views of the film morphology after alternate sputtering of Pd and Au, followed by Pt sputtering, at different times. ●C, ●Pd, ●Pt, ●Au

Magnetron sputtering is indeed capable of depositing thin catalyst films in both modes. The simulated deposition corresponds to the following experimental conditions, determining the input data for the MD simulations: sputtering argon gas pressure of 1 Pa and target-to-substrate distance of 7 cm. The MD simulations are based on the EAM potentials [32] for metals, Tersoff potential for carbon support [41-42] and Lennard-Jones mixing rules for metal-carbon interactions [17, 22].

For the co-sputtering / simultaneous deposition condition (Fig. 9), a Pt core in the catalyst is observed, surrounded by a PdAu shell. This is in agreement with predicted surface energies and heat of solutions for elements interacting with EAM potentials [30]. In order to obtain Pt in the outer shell, it is thus mandatory to carry out alternated deposition: first the PdAu core is deposited, with random deposition of both elements during a fixed time, followed by Pt deposition. In the simulation, we allowed for 4000 Pd and Au atoms to be deposited, and for 2000 Pt atoms (see Figure 10). So Pt is effectively producing a shell around the PdAu core. It is observed, however, that some Au atoms are diffusing to the Pt shell creating an Au filament. Moreover, the PdAu core consists of a Pd zone separated by Au thin “walls”. This results from coalescence of PdAu particles, keeping the Au shell unchanged. These results are currently compared to the behavior of experimentally sputtered PdPtAu trimetallic catalyst used in fuel cells. It is observed that the catalyst function degrades with time. This degradation mechanism seems to be related to the fact that Au is migrating through the Pt-shell, to form an outer Au-shell, preventing Pt efficiency.

Such examples clearly demonstrate the interest and need in closely studying nanoscale mechanisms of multimetallic catalyst growth.

5. Conclusions

In this contribution we reviewed MD simulations on catalyst formation through plasma sputter deposition. Such simulations provide insight into processes at the molecular scale and often provide information complementary to experiments. Care should be taken, however, when conducting such simulations regarding at least three major issues. First, the properties, capabilities and limitations of the interatomic potential used in the simulations should be well understood and its validity domain / transferability should be clearly established. Although interatomic potentials are typically fitted against ab-initio and/or experimental data, extensive testing against experiments is always mandatory. Second, the input of the MD simulations should be consistent with experiments, including for instance particle fluxes and initial velocity distributions. Third, the energy transfer and exchange during deposition should be carefully addressed in order to avoid the occurrence of unphysical events such as thermal spikes or erroneous sticking coefficients. Moreover, the choice of a realistic catalyst support (including e.g. it's morphology and structure) is essential for allowing meaningful comparison to experiments.

When these requirements are fulfilled, analysis of the nanocatalyst growth and its properties can be pursued. The magnitude of the metal-substrate interaction has been shown to play an important role, for instance in wetting of the Pt catalyst cluster on a realistic porous carbon support, allowing for direct comparison with experiments. Variation of parameters such as the kinetic energy of the impinging particles allows to highlight how cluster growth evolves and how morphology can be controlled as observed in sputter deposition experiments.

We envisage that the field will develop in the near future by the formation of new catalysts, obtained through clean processing. MD simulations may assist in this development, by addressing the molecular scale phenomena occurring during the growth process. This requires the development and use of new interatomic potentials. Second, it is likely that multimetallic catalyst with defined structure and morphology will become more popular. Here, too, MD simulations may be of use by in-silico screening of catalyst formation and catalyst properties, thereby reducing the need for costly combinatorial experiments.

Acknowledgements.

Lu Xie is gratefully acknowledged for making Pt/CNT results available.

References

[1] P.J. Kelly, R.D. Arnell, Magnetron sputtering: a review of recent developments and applications, Vacuum 56 (2000) 159-172

[2] A. Bogaerts, E. Bultinck, I. Kolev, L. Schwaederlé, K. Van Aeken, G. Buyle and D. Depla, Computer modelling of magnetron discharges, J. Phys. D: Appl. Phys. 42 194018

[3] S. Pratontep, S. J. Carroll, C. Xirouchaki, M. Streun and R. E. Palmer, Size-selected cluster beam source based on radio frequency magnetron plasma sputtering and gas condensation, Rev. Sci. Instrum. 76 (2005) 045103

[4] P. Brault, Plasma deposition of catalytic thin films: Experiments, Applications, Molecular modeling, Surf. Coat. Technol. 205 (2011) S15-S23

[5] A. Chen, P. Holt-Hindle, Platinum-based nanostructured materials: synthesis, properties, and applications, Chem. Rev. 110 (2010) 3767-3804

[6] Fuel Cell Catalysis (Wiley, Ed. M. T. Koper, Hoboken NJ, 2009)

[7] B. Alder, T. Wainwright, 1958 Transport processes in statistical mechanics, Ed. I. Prigogine, Interscience Publishers, New York) pp. 97-131

[8] B.J. Alder and T.E. Wainwright 1959 Studies in Molecular Dynamics. I. General Method, J. Chem. Phys., 31(2), 459- 466.

[9] M.P. Allen and D.J. Tildesley, 1987. Computer Simulations of Liquids, New York: Oxford University Press.

[10] D. Frenkel and B. Smit, 2001. Understanding Molecular Simulation, Orlando: Academic Press.

[11] J.M. Haile, 1992. Molecular Dynamics Simulations, New York: John Wiley and Sons.

[12] D.C. Rapaport, 1995. The Art of Molecular Dynamics Simulations, Cambridge: Cambridge University Press.

[13] V Georgieva, I T. Todorov, A Bogaerts, Molecular dynamics simulation of oxide thin film growth: Importance of the inter-atomic interaction potential, Chemical Physics Letters 485 (2010) 315–319

[14] V. Georgieva, A. F. Voter, and A Bogaerts, Understanding the Surface Diffusion Processes during Magnetron Sputter-Deposition of Complex Oxide Mg-Al-O Thin Films, Cryst. Growth Des. 11 (2011) 2553–2558

[15] L. Xie, P. Brault, A.-L. Thomann, L. Bedra, Molecular dynamics simulation of binary ZrxCu100-x metallic glass thin film growth, Appl. Surf. Sci. 274 (2013) 164 – 170

[16] L. Xie, P. Brault, A.-L. Thomann, J.-M. Bauchire, AlCoCrCuFeNi high entropy alloy cluster growth and annealing on silicon: A classical molecular dynamics simulation study, Appl. Surf. Sci. 285P (2013) 810-816

[17] L. Xie, P. Brault, C. Coutanceau, A. Caillard, J. Berndt, E. Neyts, Efficient amorphous platinum catalyst cluster growth on porous carbon: A combined Molecular Dynamics and experimental study, Appl. Cat. B, 62 (2015) 21 - 26

[18] H. M. Urbassek, Molecular-dynamics simulation of sputtering 122, (1997) 427–441

[19] H. Haberland, Z. Insepov, and M. Moseler, Molecular dynamics simulation of thin film formation by energetic cluster impact (ECI), Z. Phys. D 26 (1993) 229-231

[20] H. Haberland, Z. Insepov, and M. Moseler, Molecular-dynamics simulation of thin-film growth by energetic cluster impact, Phys. Rev. B 51 (1995) 11061

[21] E.C. Neyts and A.Bogaerts, Understanding plasma catalysis through modelling and simulation - a review, J. Phys. D: Appl. Phys., 47, 224010 (2014).

[22] D. Graves, P. Brault, Molecular dynamics for low temperature plasma-surface interaction studies, J. Phys. D 42 (2009) 194011

[23] W. Thompson, II. The energy spectrum of ejected atoms during the high energy sputtering of gold, Philosophical Magazine 18 (1968) 377-414

[24] Theory of Sputtering. I. Sputtering Yield of Amorphous and Polycrystalline Targets, Phys. Rev. 184 (1969) 383

[25] K. Meyer, I.K. Schuller, C.M. Falco, Thermalization of sputtered atoms, Journal of Applied Physics 52 (1981) 5803-5805

[26] A. Gras-Marti, J.A. Valles-Abarca, Slowing down and thermalization of sputtered particle fluxes: Energy distributions, Journal of Applied Physics 54 (1983) 1071-1075

[27] S. J. Plimpton and A. P. Thompson Computational aspects of many-body potentials, MRS Bulletin 37 (2012) 513-521

[28] K. Albe, K. Nordlund, and R. S. Averback, Modeling the metal-semiconductor interaction: Analytical bond-order potential for platinum-carbon, Phys. Rev. B 65 (2002) 195124

[29] S. Huygh, A. Bogaerts, A. C. T. van Duin, E. C. Neyts, Development of a ReaxFF reactive force field for intrinsic point defects in titanium dioxide, Comput. Mater. Sci. 95 (2014) 579-591

[30] S. M. Foiles, M. I. Baskes, M. S. Daw, Embedded-atom-method functions for the fcc metals Cu, Ag, Au, Ni, Pd, Pt, and their alloys, Phys. Rev. B 33 (1986) 7983-799; Erratum: Phys. Rev. B 37 (1988) 10378

[31] S.M. Foiles, M.I. Baskes Contributions of the embedded-atom method to materials science and engineering, MRS Bulletin, 37 (2012) 485-491.

[32] X. W. Zhou, R. A. Johnson, and H. N. G. Wadley, Misfit-energy-increasing dislocations in vapor-deposited CoFe/NiFe multilayers, Phys. Rev. B 69 (2004) 144113

[33] Z.-B. Lin, R. -A. Johnson, and L.-V. Zhigilei, Computational study of the generation of crystal defects in a bcc metal target irradiated by short laser pulses, Physical Review B 77 (2008) 214108

[34] M. W. Finnis, J. E. Sinclair, A simple empirical N-body potential for transition metals, Philos. Mag. A 50 (1984) 45-55.

[35] A. P. Sutton , J. Chen,. Long-range Finnis-Sinclair potentials (1990) Philos. Mag. Lett. 61 139.

[36] F. Cleri, V. Rosato, Tight-binding potentials for transition metals and alloys Phys. Rev. B 48 (1993) 22.

[37] G. Treglia, B. Legrand, F. Ducastelle, A. Saul, C. Gallis, I. Meunier, C. Mottet, A. Senhaji, Alloy surfaces: segregation, reconstruction and phase transitions, Comp. Mat. Sci. 15 (1999) 196-235

[38] C. Goyhenex, H. Bulou, Theoretical insight in the energetics of Co adsorption on a reconstructed Au(111) substrate, Phys. Rev. B63 (2001) 235404.

[39] P. Brault, A. Caillard, C. Charles, R. Boswell, D. B. Graves, Platinum nanocluster growth on vertically aligned carbon nanofiber arrays: sputtering experiments and molecular dynamics simulations, Appl. Surf. Sci. 263 (2012) 352-356

[40] J. Tersoff, Modeling solid-state chemistry: Interatomic potentials for multicomponent systems, Physical Review B, 39 (1989) 5566-5568.

[41] J. Tersoff, Empirical interatomic potential for carbon, with applications to amorphous carbon, Physical Review Letters, 61 (1988) 2879-2882.

[42] J. Tersoff, New empirical approach for the structure and energy of covalent systems, Physical Review B, 37 (1988) 6991.

[43] D. W. Brenner. Empirical potential for hydrocarbons for use in simulating the chemical vapor deposition of diamond films. Physical Review B, 42(15):9458–9471, 1990.

[44] D. W. Brenner, O. A. Shenderova, J. A Harrison, S. J. Stuart, B. Ni, and S. B. Sinnott, A second-generation reactive empirical bond order (REBO) potential energy expression for hydrocarbons. Journal of Physics: Condensed Matter, 14(4):783–802, 2002.

[45] A. C. T. van Duin, S. Dasgupta, Francois Lorant, and W. A. Goddard III, ReaxFF: A Reactive Force Field for Hydrocarbons, J. Phys. Chem. A 2001, 105, 9396-9409

[46] P. Vashishta, R. K. Kalia, A. Nakano, W. Li, I. Ebbsjo, in: Amorphous Insulators and Semiconductors (Eds. M. F. Thorpe, M. I. Mitkova), Kluwer, The Netherlands, 1997, pp151-213

[47] P. K. Naicker, P. T. Cummings, H. Zhang, and J. F. Banfield, Characterization of titanium dioxide nanoparticles using molecular dynamics simulations, J. Phys. Chem. B 109 (2005) 15243-15249

[48] L.J. Vernon, Roger Smith, S.D. Kenny, Modelling of deposition processes on the TiO2 rutile (110) surface, Nuclear Instruments and Methods in Physics Research B 267 (2009) 3022–3024

[49] L. Vernon, S.D. Kenny, Roger Smith, Growth of TiO2 surfaces following low energy (<40 eV) atom and small cluster bombardment, Nuclear Instruments and Methods in Physics Research B 268 (2010) 2942–2946

[50] A. Hallil, R. Tétot, F. Berthier, I. Braems, and J. Creuze, Use of a variable-charge interatomic potential for atomistic simulations of bulk, oxygen vacancies, and surfaces of rutile TiO_2, Phys. Rev. B 73 (2006) 165406

[51] Y.-T. Cheng, T.-R. Shan, T. Liang, R. K. Behera, S. R. Phillpot and S. B. Sinnott, A charge optimized many-body (comb) potential for titanium and titania, J. Phys.: Condens. Matter 26 (2014) 315007

[52] F. H. Streitz and J. W. Mintmire, Electrostatic potentials for metal-oxide surfaces and interfaces Phys. Rev. B 50 (1994) 11996

[53] J. E. Angelo, M. I. Baskes, Interfacial studies using the EAM and MEAM. Interface Science 4 (1996) 47–63.

[54] M. I. Baskes, Modified embedded atom method calculations of interfaces, Sandia Reports 96 (1996) 8484

[55] B. W. H. van Beest, G. J. Kramer, and R. A. van Santen, Force fields for silicas and aluminophosphates based on ab initio calculations, Phys. Rev. Lett. 64 (1990) 1955

[56] P. Tangney and S. Scandolo, An ab initio parametrized interatomic force field for silica, J. Chem. Phys. 117(2002) 8898

[57] D. Herzbach, K. Binder and M. H. Müser, Comparison of model potentials for molecular-dynamics simulations of silica, J. Chem. Phys. 123 (2005) 124711

[58] J. Yu, S. B. Sinnott, and S. R. Phillpot, Charge optimized many-body potential for the Si/SiO_2 system, Phys. Rev. B 75 (2007) 085311

[59] S. Munetoh, T. Motooka, K. Moriguchi, A. Shintani., Interatomic potential for Si–O systems using Tersoff parameterization, Comp. Mat. Sci., 39 (2007) 334-339

[60] V Georgieva, M Saraiva, N Jehanathan, O I Lebelev, D Depla and A Bogaerts, Sputter-deposited Mg–Al–O thin films: linking molecular dynamics simulations to experiments, J. Phys. D: Appl. Phys. 42 (2009) 065107

[61] X.W. Zhou, H.N.G. Wadley, A potential for simulating the atomic assembly of cubic AB compounds, Computational Materials Science 39 (2007) 541–551

[62] J. K. Nørskov, T. Bligaard, J. rRossmeisl and C. H. Christensen, towards the computational design of solid catalysts, Nature Chemistry 1 (2009) 37-46

[63] S. Y. Liem, K. Y. Chan, Simulation study of platinum adsorption on graphite using the Sutton-Chen potential, Surf. Sci. 328 (1995) **1995**, 328, 119

[64] S. Y. Liem, K. Y. Chan, Effective pairwise potential for simulations of adsorbed platinum. Mol. Phys. 86 (1995) 939.

[65] S.-P. Ping, P. B. Balbuena, Platinum nanoclusters on graphite substrates: a molecular dynamics study, Molecular Physics 100 (2002) 2165-2174

[66] B. H. Morrow, A. Striolo, Assessing how metal–carbon interactions affect the structure of supported platinum nanoparticles. *Mol. Simulat*. **2009**, *35*, 795.

[67] C. K. Acharya, D. I. Sullivan, C. H. Turner, Characterizing the interaction of Pt and PtRu clusters with boron-doped, nitrogen-doped, and activated carbon: Density functional theory calculations and parameterization. *J. Phys. Chem. C*. **2008**, *112*, 13607.

[68] W. Somers, A. Bogaerts, A.C.T. van Duin, E. Neyts, Plasma species interacting with nickel surfaces : toward an atomic scale understanding of plasma-catalysis, The journal of physical chemistry: C 116 (2012) 20958-20965

[69] W. Somers, A. Bogaerts, A. C. T. van Duin, S. Huygh, K. M. Bal, E. C. Neyts, Temperature influence on the reactivity of plasma species on a nickel catalyst surface: An atomic scale study. *Cat. Today* 211 (2013) 131-136.

[70] W. Somers, A. Bogaerts, A. C. T. van Duin, E. C. Neyts, Interactions of plasma species on nickel catalysts: A reactive molecular dynamics study on the influence of temperature and surface structure. *Appl. Catal. B: Environ.* 154-155 (2014) 1-8.

[71] K. D. Nielson, A. C van Duin, J. Oxgaard, W. Q. Deng, W. A. Goddard III, Development of the ReaxFF reactive force field for describing transition metal catalyzed reactions, with application to the initial stages of the catalytic formation of carbon nanotubes, J Phys Chem A 109 (2005) 493-499.

[72] E. C. Neyts, Y. Shibuta, A. C. T. van Duin, A. Bogaerts, Catalyzed growth of carbon nanotube with definable chirality by hybrid molecular dynamics – force biased Monte Carlo simulations. *ACS Nano* 4 (2010) 6665-6672.

[73] E. C. Neyts, A. C. T. van Duin, A. Bogaerts, Insights in the plasma-assisted growth of carbon nanotubes through atomic scale simulations: Effect of electric field. Journal of the American Chemical Society 134 (2012) 1256-1260.

[74] E. C. Neyts, K. Ostrikov, Z. J. Han, S. Kumar, A. C. T. van Duin, A. Bogaerts, Defect healing and enhanced nucleation of carbon nanotubes by low-energy ion bombardment, *Phys. Rev. Lett.* 110 (2013) 065501.

[75] K. Kayhania, K. Mirabbaszadeha, P. Nayebib, A. Mohandesia, Surface effect on the coalescence of Pt clusters: A molecular dynamics study, Applied Surface Science 256 (2010) 6982–6985

[76] S. M. Levine and S. H. Garofalini, Computer simulation of interactions of model Pt particles and films with the silica surface, J. Chem. Phys. 88, 1242 (1988)

[77] A. Endou, K. Teraishi, K. Yajima, K. Yoshizawa, N. Ohashi, S. Takami, M. Kubo, A. Miyamoto and E. Broclawik, Potential Energy Surface and Dynamics of Pd/MgO(001) System as Investigated by Periodic Density Functional Calculations and Classical Molecular Dynamics Simulations, Jpn. J. Appl. Phys. 39 (2000) 4255

[78] N. C. Hernandez and J. Fernandez Sanz, Molecular Dynamics Simulations of Pd Deposition on the α-Al2O3 (0001) Surface, J. Phys. Chem. B 105 (2001) 12111-12117

[79] X. W. Zhou, R. A. Johnson, and H. N. G. Wadley, A molecular dynamics study of nickel vapor deposition: temperature, incident angle, and adatom energy effects, Acta mater 45 (1997) 1513-1524

[80] S Inoue, Y Matsumura, Molecular dynamics simulation of physical vapor deposition of metals onto a vertically aligned single-walled carbon nanotube surface, Carbon 46 (2008) 2046-2052

[81] L. Xie, Simulations of plasma sputtering deposition and thin film growth, Ph D thesis manuscript (2013) Université d'Orléans, France. URL: https://tel.archives-ouvertes.fr/tel-00933201/document

[82] P. Brault, A. Caillard, S. Baranton, M. Mougenot, S. Cuynet, C. Coutanceau, One-step synthesis and chemical characterization of Pt C nanowire composites by plasma sputtering, ChemSusChem. 6 (2013) 1168-1171

[83] A. Caillard, P. Brault, J. Mathias, C. Charles, R. Boswell, T. Sauvage, Surf. Coat.Technol. 200 (2005) 391

[84] P. Brault, C. Josserand, J.M. Bauchire, A. Caillard, C. Charles, R.W. Boswell, Phys.Rev. Lett. 102 (2009) 045901.

[85] K. J.Hansen, T. Worren, S.Stempel, E. Laegsgaard, M. Bäumer,; H.-J. Freund, F. Besenbacher, I. Stensgaard, Palladium nanocrystals on Al 2 O 3: structure and adhesion energy, Phys. Rev. Lett. 83 (1999) 4120.

[86] A. Sandell, J. Libuda, M. Bäumer, H.-J. Freund, Metal deposition in adsorbate atmosphere: growth and decomposition of a palladium carbonyl-like species, Surf. Sci. 346 (1996) 108.

[87] Guofeng Wang, M.A. Van Hovea, P.N. Ross, M.I. Baskes, Quantitative prediction of surface segregation in bimetallic Pt–M alloy nanoparticles (M = Ni, Re, Mo), Progress in Surface Science 79 (2005) 28-45

[88] W. A. Goddard III, A. C. T. van Duin, K. Chenoweth, M.-J. Cheng, S. Pudar, J. Oxgaard, B. Merinov, Y. H. Jang and P. Persson, Development of the ReaxFF reactive force field for mechanistic studies of catalytic selective oxidation processes on $BiMoO_x$, Top. Catal. 38 (2006) 93-103

[89] K. Chenoweth, A. C. T. van Duin, W. A. Goddard III, The ReaxFF Monte Carlo reactive dynamics method for predicting atomistic structures of disordered ceramics application to the Mo3VOx catalyst, Angew. Chem. Int. Ed. 48 (2009) 7630-7634.

[90] B. Fang, B. N. Wanjala, J. Yin, R. Loukrakpam, J. Luo, X. Hu, J. Last, C.-J. Zhong, Electrocatalytic performance of Pt-based trimetallic alloy nanoparticle catalysts in proton exchange membrane fuel cells, Int. J. Hydrogen Energy 37 (2012) 4627-4632

[91] J. Barroso, A.R. Pierna, T.C. Blanco, N. Ruiz, Trimetallic amorphous catalyst with low amount of platinum: Comparative study for ethanol, bioethanol and CO electrooxidation,

[92] B. Lia, S. Hwa Chan, PtFeNi tri-metallic alloy nanoparticles as electrocatalyst for oxygen reduction reaction in proton exchange membrane fuel cells with ultra-low Pt loading, Int. J. Hydrogen Energy 38 (2013) 3338–3345